Geophysical Journal International

*Geophys. J. Int.* (2019) **217,** 2081–2096
Advance Access publication 2019 March 19
GJI Seismology

doi: 10.1093/gji/ggz144

# Simulation of Stoneley wave reflection from porous formation in borehole using FDTD method

Weiming Ou and Zhuwen Wang

*College of Geo-Exploration Science and Technology, Jilin University, Changchun* 130021*, China. E-mail: wangzw@jlu.edu.cn*

Accepted 2019 March 18. Received 2018 March 10; in original form 2018 August 20



## SUMMARY

Stoneley waves propagating in a borehole will produce reflected waves when they encounter a porous formation. In previous studies, the simplified Biot–Rosenbaum theory is used to calculate the Stoneley wave reflection coefficient for porous formations. Such simplified theory ignores the effect of formation frame elasticity, thus cannot obtain accurately the Stoneley wave reflection for the porous formation with small stiffness. In this study, to take the effect of formation frame elasticity into account, we use the Biot's theory in the low-frequency limit to simulate the Stoneley wave reflection by employing the velocity-stress finite-difference time-domain (FDTD) method. In addition, as permeability of the formation varies in the axial direction, and the viscosity of the pore fluid also changes in a radial direction due to mud invasion, it is difficult to use the simplified theory to calculate the reflection coefficient of the Stoneley wave in such heterogeneous cases. Therefore, this study first investigates the effect of the formation permeability heterogeneity on Stoneley wave reflection coefficient by this FDTD method.

The FDTD method is verified by a comparison with the real axis integration method with respect to the Stoneley wave propagation in a borehole surrounded by a homogeneous porous formation. The reflection coefficient obtained by the FDTD method is smaller than that using the simplified theory, which shows that elasticity of the formation frame affects Stoneley wave reflection: the effect of elasticity on the reflection coefficient is greater when the formation frame is less rigid or when the porosity and permeability of the formation are lower. According to the simulation results of the FDTD method, a modified simplified theory which can improve the calculation accuracy of Stoneley wave reflection coefficient is proposed. Furthermore, the effects of the permeability heterogeneity on the Stoneley wave reflection are investigated: the reflection coefficient peaks change when permeability alters in an axial direction and the peak interval increases. For the mud invasion model, the reflection coefficient is almost identical to that of the homogeneous model, which has the same permeability as the borehole wall of the mud invasion model.

**Key words:** Permeability and porosity; Numerical modelling; Acoustic properties; Wave propagation; Guide waves.

## 1 INTRODUCTION

Stoneley waves are particularly sensitive to permeable formations, and they can well reflect the characteristics of porous formations around boreholes. A considerable amount of research has been conducted on Stoneley wave propagation in boreholes surrounded by porous formations (Rosenbaum 1974; Cheng *et al.* 1987; Chang *et al.* 1988; Tang *et al.* 1991a; Karpfinger *et al.* 2010). In this respect, Rosenbaum (1974) used Biot's theory (Biot 1956a,b, 1962) to simulate the logging of acoustic waves within the porous media. However, the Biot–Rosenbaum method (Rosenbaum 1974) is found to be particularly time-consuming when using Stoneley waves of well logging data to invert formation permeability (Tang & Cheng 1996). Tang *et al.* (1991a) proposed the simplified Biot–Rosenbaum theory (hereafter referred to as the 'simplified theory'), which was found to be very convenient and highly efficient when used to solve the propagation problem of low-frequency Stoneley waves in permeable boreholes. Based on the simplified theory (Tang *et al.* 1991a), Zhao *et al.* (1993) used the finite-difference method to study the effects of a heterogeneous permeable porous formation on Stoneley wave propagation.

The simplified theory of Tang *et al.* (1991a) has since been often applied in studies of Stoneley wave reflections from porous formations. Tang & Cheng (1993) applied the simplified theory to study the reflection of Stoneley waves in permeable formations and obtained a

calculation formula for the reflection coefficient. Furthermore, Bakulin *et al.* (2005) used the simplified theory to investigate the reflection response of Stoneley waves from various finite-size poroelastic structures. Alexandrov *et al.* (2007) extended the simplified theory to a radial inhomogeneous formation and studied the reflection of Stoneley waves in the casing borehole.

However, compared with the Biot–Rosenbaum theory (Rosenbaum 1974), the simplified theory of Tang *et al.* (1991a) mainly considers the influence of formation permeability and does not fully consider the coupling of pore fluid and frame elasticity. For a soft porous formation, the error of the phase velocity and attenuation of Stoneley wave calculated by the simplified theory is relatively large (Tang & Cheng 2004). Therefore, these theories that employ the simplified theory cannot accurately calculate the reflection coefficient of Stoneley waves from a porous formation with small stiffnesses frame. To obtain the accurate Stoneley wave reflection coefficient, it needs to consider the effect of the frame elasticity based on the Biot's theory (Biot 1956a,b, 1962). In addition, these studies cannot simulate Stoneley wave reflection from a heterogeneous permeable formation. In contrast, the FDTD method can deal with the problem of heterogeneity (Virieux 1986; Dai *et al.* 1995; Guan & Hu 2011; Moczo *et al.* 2014, 2019; Kristek *et al.* 2017). In the method of Dai *et al.* (1995), the heterogeneity of the porous medium is determined by the material parameters assigned to the grid position. Moczo *et al.* (2002) correctly suggested that it needed to use the effective material parameters to represent the interface between two media. Guan & Hu (2011) and Moczo *et al.* (2019) obtained effective medium parameters on the interface between two poroelastic media according to the boundary conditions. Compared with the parameter averaging technique of Guan & Hu (2011), the discrete representation of Moczo *et al.* (2019) has higher accuracy and can model the interface of any shape and position in the grid.

Based on Biot's theory (Biot 1956a,b, 1962), several FDTD algorithms have recently been applied to simulate the propagation of elastic waves in porous media (e.g. Zhu & Mc Mechan 1991; Zeng & Liu 2001; Zeng *et al.* 2001; Moczo *et al.* 2019; see Moczo *et al.* 2019 for a recent review of the FDTD modelling approaches). These algorithms use static permeability and are effective at very low frequencies. In this case, the inertial force is much less than the viscous forces, so it can be ignored. Masson *et al.* (2006), Guan & Hu (2008) adopted dynamic permeability and approximated the frequency correction function of the viscous force in the time-domain by using Taylor expansion, thereby obtaining a new FDTD method for solving the low-frequency Biot's equations. Guan *et al.* (2009) and He *et al.* (2012, 2013) extended this FDTD method into a simulation of the acoustic logging; waveforms simulated by this FDTD method are found to be consistent with that of the RAI method, which thus proves that this FDTD method is effective. Therefore, this study employs the Biot's theory in the low-frequency limit (Masson *et al.* 2006) to simulate Stoneley wave reflection from a porous formation using this new FDTD method (Guan *et al.* 2009; Guan & Hu 2011).

First, we recall the Biot's theory in the low-frequency limit (Masson *et al.* 2006) of wave propagation in poroelastic media. We then review the FDTD scheme in modelling acoustic logs in porous formation developed by Guan & Hu (2011). Later the Stoneley wave propagation in a borehole surrounded by a homogeneous porous formation is simulated by using the staggered-grid FDTD method. Solutions of this method are then compared with the RAI method to verify our method. Stoneley wave reflection is then simulated in a variety of formations with different frame elasticities, porosities and permeabilities, and the Stoneley wave reflection coefficient of the FDTD method is compared with that of the simplified theory to investigate the effects of formation elasticity on Stoneley wave reflection. A simple scheme that can be used to correct the simplified theory is then provided. Finally, the FDTD method is used to investigate the effects of heterogeneous permeability on Stoneley wave reflection.

## 2 FORMULATION

### 2.1 Biot's equations in the low-frequency limit

The propagation of acoustic waves in a borehole can be described using Biot's theory of pore elastic wave (Biot 1956a,b, 1962). Many forms of Biot's theory exist, and we here adopt the revised theory of Auriault *et al.* (1985) and Para & Xu (1994). Assuming an $e^{-i\omega t}$ time dependence of all field quantities, the propagation equations of elastic waves in isotropic, fluid-saturated porous media is as follows:

$$-i\omega\mathbf{w} = \left(-\nabla p + \omega^2 \rho_{\mathrm{f}}\mathbf{u}\right)\kappa(\omega)/\eta, \tag{1}$$

$$\nabla\cdot\tau = -\omega^2\left(\rho\mathbf{u} + \rho_{\mathrm{f}}\mathbf{w}\right), \tag{2}$$

$$\tau = (H-2G)(\nabla\cdot\mathbf{u})\mathbf{I} + C(\nabla\cdot\mathrm{w})\mathbf{I} + G\left(\nabla\mathbf{u} + \nabla\mathbf{u}^{\mathbf{T}}\right), \tag{3}$$

$$-p = C\nabla\cdot\mathbf{u} + M\nabla\cdot\mathbf{w}, \tag{4}$$

where $\omega$ is the circular frequency, $\mathbf{u}$ is the solid phase displacement vector, $\mathbf{w}$ is the relative displacement vector of fluid and solid phase, $\tau$ is stress tensor volume, $p$ is pore fluid pressure, $\mathbf{I}$ is equivalent tensor, $\rho_{\mathrm{f}}$ is fluid density, $\eta$ is the fluid viscosity, for water $\eta = 10^{-3}\mathrm{Pa}\cdot\mathrm{s}$, $\rho$ is formation density, $G$ is the shear modulus of the porous formation and $H$, $C$ and $M$ are the porous formation moduli defined by Biot (1962).

The dynamic permeability $\kappa(\omega)$ in the eq. (1) is defined by Johnson *et al.* (1987) as follows:

$$\kappa(\omega) = \kappa_0 \left[ \left(1 - \frac{4i\omega}{m\omega_c}\right)^{1/2} - i\frac{\omega}{\omega_c} \right]^{-1}, \tag{5}$$

where $\kappa_0$ is the static Darcy permeability, $m$ is a dimensionless parameter for a porous media and $m \approx 8$. Furthermore $\omega_c = \phi\eta/(\alpha_\infty \rho_f \kappa_0)$ represents the critical frequency, which separates the low-frequency viscous flow and the high-frequency inertial force (where $\phi$ is porosity, $\alpha_\infty$ is tortuosity and $\alpha_\infty = 3$ for round pores; Tang & Cheng 2004).

Dynamic permeability is a measure of the fluid flow performance in a porous medium under dynamic fluctuation. At a low frequency ($\omega \to 0$), $\kappa(\omega)$ is close to $\kappa_0$, and the fluid motion in the pore is mainly viscous fluid motion, but as the frequency increases, the inertial forces gradually increase, and at a high frequency ($\omega \gg \omega_c$), the inertial forces control the viscous boundary layers.

A highly permeable formation that is filled with water has a static permeability $\kappa_0$ of 2 Darcy, porosity $\phi$ of 0.3 and $\omega_c = 50$ kHz can be obtained. From the formula, it is evident that $\omega_c$ is inversely proportional to $\kappa_0$. In general, the permeability of a porous formation is smaller than 2 Darcy; therefore, the $\omega_c$ of the formation is greater than 50 kHz. The frequency, $F$, of the Stoneley wave is generally less than 4 kHz and $\omega = 2\pi F \ll \omega_c$. As $|4\omega/m\omega_c| < 1$, a Taylor expansion can be used to express the first item in the square bracket of eq. (5), and this equation is (Masson *et al.* 2006)

$$\sqrt{1 - \frac{4i\omega}{m\omega_c}} = 1 - \frac{2i\omega}{m\omega_c} + \frac{2}{m^2}\left(\frac{\omega}{\omega_c}\right)^2 + o\left(\frac{\omega}{\omega_c}\right)^3. \tag{6}$$

As $\omega \ll \omega_c$, the third item on the right-hand side of formula (6) is the high-order quantity, and it can be ignored; therefore, the approximate equation of dynamic permeability is as follows:

$$\kappa(\omega) = \kappa_0 \left(1 - \frac{2i\omega}{m\omega_c} - \frac{i\omega}{\omega_c}\right)^{-1}. \tag{7}$$

Substituting eq. (7) into eq. (1) obtains

$$-i\omega\frac{\eta}{k_0}\mathbf{w} + (i\omega)^2\left(1 + \frac{2}{m}\right)\frac{\eta}{k_0\omega_c}\mathbf{w} = -\nabla p + \omega^2\rho_f\mathbf{u}. \tag{8}$$

By setting $D_1 = (1 + 2/m)\eta/(\kappa_0\omega_c)$, and $D_2 = \eta/\kappa_0$, we obtain

$$(D_2 - i\omega D_1)\,\mathbf{v}_w = -\nabla p + i\omega\rho_f\mathbf{v}_u, \tag{9}$$

where $\mathbf{v}_w = -i\omega\mathbf{w}$ is the velocity vector of the fluid relative to the solid phase and $\mathbf{v}_u = -i\omega\mathbf{u}$ is the velocity vector of solid phase. Biot's eqs (2)–(4) and (9) are converted into time-domain equations relating to velocity and stress, and these new equations are expressed as follows (Masson *et al.* 2006; Guan *et al.* 2009; Guan & Hu 2011),

$$D_1\frac{\partial\mathbf{v}_w}{\partial t} + D_2\mathbf{v}_w + \rho_f\frac{\partial\mathbf{v}_u}{\partial t} = -\nabla p, \tag{10}$$

$$\nabla\cdot\tau = \rho\frac{\partial\mathbf{v}_u}{\partial t} + \rho_f\frac{\partial\mathbf{v}_w}{\partial t}, \tag{11}$$

$$\frac{\partial\boldsymbol{\tau}}{\partial t} = (H - 2G)(\nabla\cdot\mathbf{v}_u)\mathbf{I} + C(\nabla\cdot\mathbf{v}_w)\mathbf{I} + G(\nabla\mathbf{v}_u + \mathbf{v}_u\nabla), \tag{12}$$

$$\frac{\partial p}{\partial t} = -(C\nabla\cdot\mathbf{v}_u + M\nabla\cdot\mathbf{v}_w). \tag{13}$$

### 2.2 Equations within the cylindrical coordinate system

The borehole is a cylinder; therefore, to facilitate separation of the elastic wave field equation within the porous formation, it is necessary to transform the eqs (10)–(13) into equations within the cylindrical coordinate system. Because the model is axisymmetric, $\partial/\partial\theta$ is zero (Randall *et al.* 1991). Thus, for a monopole source, eqs (10)–(13) are rewritten in cylindrical coordinates as

$$D_1 v_{wr,\,t} + D_2 v_{wr} + \rho_f v_{ur,\,t} = -P_{,\,r}, \tag{14.1}$$

$$D_1 v_{wz,\,t} + D_2 v_{wz} + \rho_f v_{uz,\,t} = -P_{,\,z}, \tag{14.2}$$

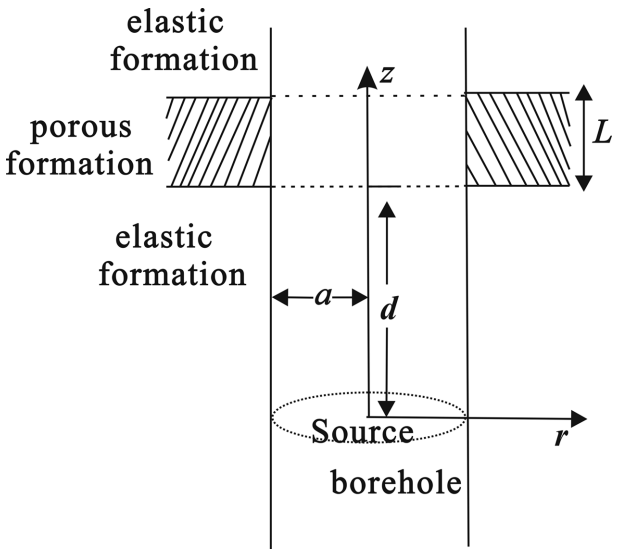


**Figure 1.** Schematic diagram of a horizontal porous formation across a borehole on the $r$–$z$ plane.

$$\tau_{rr,r} + \tau_{rz,z} + \frac{\tau_{rr} - \tau_{\theta\theta}}{r} = \rho v_{ur,\ t} + \rho_f v_{wr,\ t}, \tag{14.3}$$

$$\tau_{rz,r} + \tau_{zz,z} + \frac{\tau_{rz}}{r} = \rho v_{uz,\ t} + \rho_f v_{wz,\ t}, \tag{14.4}$$

$$\tau_{rr,t} = (H - 2G)\left(\frac{v_{ur}}{r} + v_{uz,\ z}\right) + H v_{ur,\ r} + C\left(v_{wr,\ r} + \frac{v_{wr}}{r} + v_{wz,\ z}\right), \tag{14.5}$$

$$\tau_{zz,t} = (H - 2G)\left(\frac{v_{ur}}{r} + v_{ur,\ r}\right) + H v_{uz,\ z} + C\left(v_{wr,\ r} + \frac{v_{wr}}{r} + v_{wz,\ z}\right), \tag{14.6}$$

$$\tau_{\theta\theta,t} = H\frac{v_{ur}}{r} + (H - 2G)(v_{uz,\ z} + v_{ur,\ r}) + C\left(v_{wr,\ r} + \frac{v_{wr}}{r} + v_{wz,\ z}\right), \tag{14.7}$$

$$\tau_{rz,t} = G(v_{uz,\ r} + v_{ur,\ z}), \tag{14.8}$$

$$p_{,\ t} = -C\left(v_{ur,\ r} + \frac{v_{ur}}{r} + v_{uz,\ z}\right) - M\left(v_{wr,\ r} + \frac{v_{wr}}{r} + v_{wz,\ z}\right). \tag{14.9}$$

## 3 The FDTD Scheme

Fig. 1 presents a schematic diagram of a horizontal porous formation across a borehole on the $r$–$z$ plane. The borehole is full filled with fresh water, its wall is open and there is no mud cake. The monopole acoustic source is located at the centre of the borehole, and the source is at the origin of the cylindrical coordinate system. The $z$ axis and the borehole axis are coincident, and the $r$ axis is pointing in the radial direction. The horizontal porous formation is perpendicular to the borehole axis and is sandwiched between two identical elastic formations. The distance between the lower surface of the porous formation and the source is $d$ ($d = 2$ m), and the thickness of the formation is $L$. The borehole radius is $a$ and $a = 0.1$ m. As the formation is axisymmetric, the $r$–$z$ plane can be used to simplify the equation.

Guan & Hu (2011) proposed a parameter averaging technique in FDTD method of simulating elastic waves in a combined structure with solid, fluid and porous subregions. This parameter averaging technique cannot only be used for the porous–porous formation interface, but also for fluid–porous and solid–porous interfaces. As shown in Fig. 1, the model consists of porous, elastic and fluid media. Therefore, we use the FDTD method presented by Guan & Hu (2011) to simulate the Stoneley wave propagation in the borehole.

To facilitate the application of the FDTD scheme, eq. (14.3) for $v_{ur,t}$ and eq. (14.4) for $v_{uz,t}$ are substituted into eqs (14.1) and (14.2), respectively. And eqs (14.1) and (14.2) can be rewritten as

$$D_2 v_{wr} + (D_1 - \frac{\rho_f^2}{\rho})v_{wr,t} = -P_{,\ r} - \frac{\rho_f}{\rho}\left(\tau_{rr,r} + \tau_{rz,z} + \frac{\tau_{rr} + \tau_{\theta\theta}}{r}\right), \tag{15.1}$$

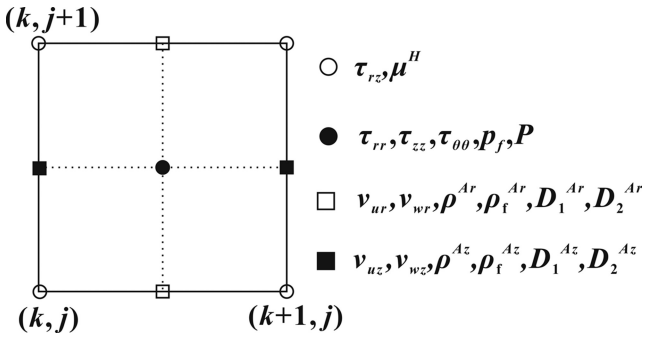


**Figure 2.** Positions of the field quantities and parameters (material parameters and averaged material parameters) in FD staggered grid in the cylindrical coordinates. For models with heterogeneous media, the interfaces between two different media are defined by the thin solid lines.

$$D_2 v_{wz} + (D_1 - \frac{\rho_f^2}{\rho}) v_{wz,t} = -P_{,\ z} - \frac{\rho_f}{\rho}\left(\tau_{rz,r} + \tau_{zz,z} + \frac{\tau_{rz}}{r}\right). \tag{15.2}$$

As shown in Fig. 2, staggered grids (Graves 1996; Masson *et al.* 2006) are used to disperse the parameters of the media within the cylindrical coordinate system, where the variate $k$ represents the gridpoints in the $r$-direction, $j$ represents the gridpoints in the $z$-direction and the variate $P$ represents all material parameters $\rho$, $\rho_f$, $D_1$, $D_2$, $M$, $C$, $H$ and $\mu$ (Masson *et al.* 2006; Guan & Hu 2011). Parameters with superscript $Ar$ or $Az$ and $\mu^{\mathrm{H}}$ are the averaged material parameters. By defining material parameters at the same locations as the normal stress components, averaged parameters at the interface can be obtained from material parameters (Chang & Randall 1988; Graves 1996; Guan & Hu 2011). These averaged parameters are used to calculate the equations of the elastic wave propagation in the porous media. The grid sizes in the $r$-direction and $z$-direction are $\Delta r$ and $\Delta z$, respectively, and $\Delta r = \Delta z$ in this model.

To eliminate the false reflected waves generated by the model boundary, the non-splitting perfectly matched layer (NPML) is applied (Wang & Tang 2003). The trapezoidal integration rule used in the NPML method for equally spaced abscissas is of second-order accuracy (Wang & Tang 2003). Therefore, we apply the second-order central difference approximations in time and space, and the equations of the elastic wave propagation in the porous media are

$$\left[D_2^{Ar}\frac{v_{wr}^{n+1/2}+v_{wr}^{n-1/2}}{2} + \left(D_1^{Ar} - \frac{\left(\rho_f^{Ar}\right)^2}{\rho^{Ar}}\right)\frac{v_{wr}^{n+1/2}-v_{wr}^{n-1/2}}{\Delta t}\right]_{(k,j+1/2)} = \left[-L_r p^n - \frac{\rho_f^{Ar}}{\rho^{Ar}}\left(L_r\tau_{rr}^n + L_z\tau_{rz}^n + \frac{\left(\tau_{rr}^n-\tau_{\theta\theta}^n\right)^{Ar}}{r_k}\right)\right]_{(k,j+1/2)}, \tag{16}$$

$$\left[D_2^{Az}\frac{v_{wz}^{n+1/2}+v_{wz}^{n-1/2}}{2} + \left(D_1^{Az} - \frac{\left(\rho_f^{Az}\right)^2}{\rho^{Az}}\right)\frac{v_{wz}^{n+1/2}-v_{wz}^{n-1/2}}{\Delta t}\right]_{(k+1/2,j)} = \left[-L_z p^n - \frac{\rho_f^{Az}}{\rho^{Az}}\left(L_r\tau_{rz}^n + L_z\tau_z^n + \frac{\left(\tau_{rz}^n\right)^{Ar}}{r_{k+1/2}}\right)\right]_{(k+1/2,j)}, \tag{17}$$

$$\left[\rho^{Ar}\frac{v_{ur}^{n+1/2}-v_{ur}^{n-1/2}}{\Delta t}\right]_{(k,j+1/2)} = \left[L_r\tau_{rr}^n + L_z\tau_{rz}^n + \frac{\left(\tau_{rr}^n-\tau_{\theta\theta}^n\right)^{Ar}}{r_k} - \rho_f^{Ar}\frac{v_{wr}^{n+1/2}-v_{wr}^{n-1/2}}{\Delta t}\right]_{(k,j+1/2)}, \tag{18}$$

$$\left[\rho^{Az}\frac{v_{uz}^{n+1/2}-v_{uz}^{n-1/2}}{\Delta t}\right]_{(k+1/2,j)} = \left[L_r\tau_{rz}^n + L_z\tau_{zz}^n + \frac{\left(\tau_{rz}^n\right)^{Ar}}{r_{k+1/2}} - \rho_f^{Az}\frac{v_{wz}^{n+1/2}-v_{wz}^{n-1/2}}{\Delta t}\right]_{(k+1/2,j)}, \tag{19}$$

$$\left[\frac{\tau_{rr}^n-\tau_{rr}^{n-1}}{\Delta t}\right]_{(k+1/2,j+1/2)} = \left[(H-2\mu)\left(\frac{\left(v_{ur}^{n-1/2}\right)^{Ar}}{r_{k+1/2}} + L_z v_{uz}^{n-1/2}\right) + HL_r v_{ur}^{n-1/2} + C\left(\frac{\left(v_{wr}^{n-1/2}\right)^{Ar}}{r_{k+1/2}} + L_r v_{wr}^{n-1/2} + L_z v_{wz}^{n-1/2}\right)\right]_{(k+1/2,j+1/2)}, \tag{20}$$

**Table 1.** Formation frame parameters. Parameters $v_p$ and $v_s$ are the compressional and shear velocities of the dry rock; $\rho_s$ is the frame density and $K_s$ is the solid grain bulk modulus.

| | $v_p$ m s$^{-1}$ | $v_s$ m s$^{-1}$ | $\rho_s$ kg m$^{-3}$ | $K_s$ |
|---|---|---|---|---|
| Frame 1 | 6000 | 3500 | 3200 | $6.693 \times 10^{10}$ |
| Frame 2 | 4000 | 3000 | 2800 | $1.12 \times 10^{10}$ |
| Frame 3 | 3000 | 2000 | 2200 | $8.0667 \times 10^{9}$ |
| Frame 4 | 2500 | 1200 | 2200 | $9.526 \times 10^{9}$ |

$$\left[\frac{\tau_{zz}^{n}-\tau_{zz}^{n-1}}{\Delta t}\right]_{(k+1/2,j+1/2)} = \left[(H-2\mu)\left(\frac{\left(v_{ur}^{n-1/2}\right)^{Ar}}{r_{k+1/2}}+L_r v_{ur}^{n-1/2}\right)+HL_z v_{uz}^{n-1/2} +C\left(\frac{\left(v_{wr}^{n-1/2}\right)^{Ar}}{r_{k+1/2}}+L_r v_{wr}^{n-1/2}+L_z v_{wz}^{n-1/2}\right)\right]_{(k+1/2,j+1/2)}, \tag{21}$$

$$\left[\frac{\tau_{\theta\theta}^{n}-\tau_{\theta\theta}^{n-1}}{\Delta t}\right]_{(k+1/2,j+1/2)} = \left[(H-2\mu)(L_z v_{uz}^{n-1/2}+L_r v_{ur}^{n-1/2})+H\frac{\left(v_{ur}^{n-1/2}\right)^{Ar}}{r_{k+1/2}} +C\left(\frac{\left(v_{wr}^{n-1/2}\right)^{Ar}}{r_{k+1/2}}+L_r v_{wr}^{n-1/2}+L_z v_{wz}^{n-1/2}\right)\right]_{(k+1/2,j+1/2)}, \tag{22}$$

$$\left[\frac{\tau_{rz}^{n}-\tau_{rz}^{n-1}}{\Delta t}\right]_{(k,j)} = \left[\mu^{Ha}(L_r v_{uz}^{n-1/2}+L_z v_{ur}^{n-1/2})\right]_{(k,j)} \tag{23}$$

and

$$\left[\frac{p^{n}-p^{n-1}}{\Delta t}\right]_{(k+1/2,j+1/2)} = \left[-C\left(L_z v_{uz}^{n-1/2}+L_r v_{ur}^{n-1/2}+\frac{\left(v_{ur}^{n-1/2}\right)^{Ar}}{r_{k+1/2}}\right) -M\left(\frac{\left(v_{wr}^{n-1/2}\right)^{Ar}}{r_{k+1/2}}+L_r v_{wr}^{n-1/2}+L_z v_{wz}^{n-1/2}\right)\right]_{(k+1/2,j+1/2)}, \tag{24}$$

where superscripts $Ar$ and $Az$ represent arithmetic mean operators in the $r$-direction and $z$-direction, respectively. These averaged parameters are calculated by the parameter averaging technique presented by Guan & Hu (2011) as given in Appendix. The superscript $n$ is the index of time, $\Delta t$ is the time space, $L_q$ is the second-order FD operator in space ($q = r, z$) and the variate $r_k = k\Delta r$ is the radial distance.

To unify the FDTD equation, we regard the fluid media and elastic formation as the porous formation and use their parameter limits. In the fluid media, the field quantities and parameters are set as $\rho = \rho_f$, $\phi = 1$, $G = 0$, $C = M = H = K_f$, $D_1 = \rho_f$, $D_2 = 0$, $\tau = -p\mathbf{I}$ and $\mathbf{v}_w = 0$. With these parameters being substituted into eqs (11) and (12), eqs (11) and (12) can be reduced to the equations of acoustic wave in the fluid. The field quantities and parameters in the elastic formation are $\rho_f = \rho = \rho_s$, $\phi = 0$, $G = G_s$, $C = K_s$, $H = K_s + 4G_s/3$, $M = \infty$, $D_1 = \infty$, $D_2 = \infty$, $p = 0$ and $\mathbf{v_w} = 0$; thus eqs (11) and (12) can be reduced to the equations of wave in the elastic media. Where $\rho_s$ is the density of solid grain, $K_f$ is bulk modulus of fluid, $G_s$ and $K_s$ are shear modulus and bulk modulus of the solid grain, respectively. The monopole source is the same as that described by Tsang & Rader (1979) and the formula of source s($t$) in this paper is expressed as

$$s(t) = \begin{cases} \frac{1}{2}\left[1+\cos\frac{2\pi}{T_c}(t-\frac{T_c}{T_c})\right]\cos 2\pi f_0\left(t-\frac{T_c}{2}\right), & 0 \le t \le T_c \\ 0, & t > T_c \end{cases}, \tag{25}$$

where $f_0$ is the centre frequency of the source, $t$ is time and $T_c$ represents the acoustic source pulse width.

The stability condition of the FD method is $\Delta t < \Delta r/\sqrt{2}v_{max}$, where $v_{max}$ is the maximum velocity of the model (Randall *et al.* 1991). To reduce the grid dispersion error, the grid size should meet the requirement of $\Delta r \le \lambda_{min}/10$, where $\lambda_{min}$ is the shortest wavelength and $\lambda_{min} = v_{min}/f_{max}$ (Alford *et al.* 1974; Stephan *et al.* 1985). Here, $v_{min}$ is the minimum velocity of the model, and $f_{max}$ is the maximum frequency of the source in this paper as $2f_0$.

The parameters of formation frame are shown in Table 1. The elastic moduli of the rigid formation are infinite, and the elastic moduli of the Frame 1 is much larger than that of the water. Frame 1 can be considered as a rigid formation. The shear velocities of the Frames 2 and 3 are greater than that of the fluid, and formations associated with these two frames are hard formations. Similarly, the formation associated with Frame 4 is a soft formation.

## 4 Verification of the FDTD Method

To verify the FDTD method, we simulate the borehole acoustic field in a homogeneous porous formation using the FDTD method and the real axis integration (RAI) method (Schmitt 1988), respectively, and compare the waveforms calculated using these two methods. The interval

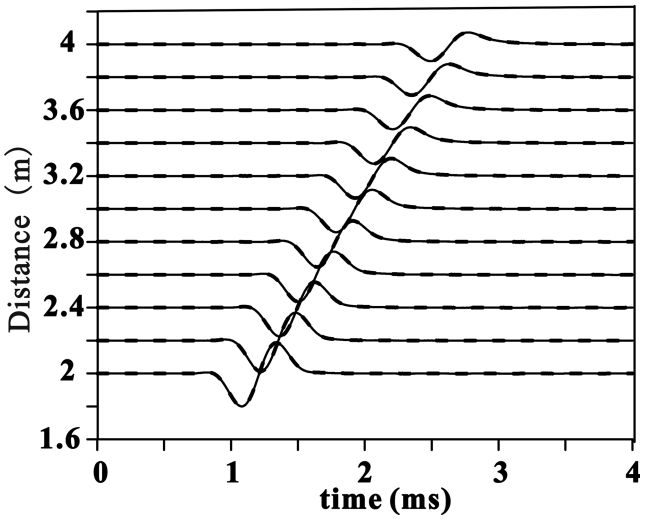


**Figure 3.** Stoneley waveforms propagating in a borehole surrounded by a homogeneous porous formation. The solid curves are waveforms obtained by the FDTD method, and dashed curves are waveforms obtained by RAI method. The interval between the receivers is 0.2 m, and the first receiver is 1 m above the source.

between the receivers is 0.2 m, and the first receiver is 1 m above the source. The centre frequency $f_0 = 2.2$ kHz is less than the cut-off frequency of the first mode pseudo-Rayleigh waves, therefore, the compressional wave and the shear wave are not excited, and only Stoneley waves are evident in the waveforms. The homogeneous porous formation's frame is Frame 2 listed in Table 1 and the physical parameters of the frame need to be converted to the parameters of a saturated fluid formation (Tang *et al.* 1991a). The porosity $\phi = 0.3$, permeability $\kappa_0 = 2$ Darcy, the FD grid size $\Delta r = 0.01$ m, the time step $\Delta t = 1 \times 10^{-6}$ s and the gridpoints in the radial direction and axial direction are 128 and 640, respectively. The computer program uses parallel computing technology based on the Graphics Processing Unit (Abbreviation for GPU), which has a computing power of 6.1, and the calculation time of the FDTD method is about 14 s.

Fig. 3 shows the waveforms of Stoneley waves propagating in a borehole surrounded by a homogeneous porous formation. The waveform recorded by the receiver represents the fluid pressure $p$ in the borehole. The solid curves are waveforms obtained using the FDTD method, and the dashed curves are waveforms obtained using the RAI method. The waveforms simulated by the two methods match very well, which verifies the FDTD method used in this study. As the permeability of formations is generally smaller than 2 Darcy, the waveforms simulated by the FDTD method are more accurate. Because of the discrete Fourier transform of the RAI method and the discrete FDTD grids, there are small differences in the amplitudes of the waveforms. The amplitude of the waveform decreases as the source distance increases, and the amplitude of Stoneley waves attenuate significantly because the energy of the wave is brought into the porous formation by slow waves.

## 5 Comparison between FDTD method and simplified theory

### 5.1 Simplified theory

The effects of formation permeability on Stoneley waves are mainly realized through the propagation mechanism of slow waves. Tang *et al.* (1991a) developed a simplified Biot–Rosenbaum theory, which divides the interaction between Stoneley waves and porous formation into two parts: the first part is the interaction between Stoneley waves and the equivalent elastic formation without slow waves, and the second part is the interaction between Stoneley waves and porous fluid flow of the formation. On the basis of this simplified theory, Tang & Cheng (1993) studied the reflection of Stoneley waves generated by the porous formation in the borehole and determined calculation formulas for the reflection coefficient $r(\omega)$ of the Stoneley wave in the frequency domain as follows:

$$k_2 = \sqrt{k_{e+}^2 + \frac{2i\rho_f\omega\kappa(\omega)}{a\eta}\sqrt{\frac{-i\omega}{D}}\frac{K_1\left(a\sqrt{-i\omega/D}\right)}{K_0\left(a\sqrt{-i\omega/D}\right)}}, \tag{26a}$$

$$k_e = \omega\sqrt{\frac{1}{v_f^2} + \frac{\rho_f}{\rho_s v_{se}^2}}, \tag{26b}$$

$$k_1 = \omega\sqrt{\frac{1}{v_f^2} + \frac{\rho_f}{\rho_s v_{s1}^2}}, \tag{26c}$$

$$G = (k_1 + k_2)^2 e^{-ik_2 L} - (k_1 - k_2)^2 e^{-ik_1 L}, \tag{26d}$$

$$r(\omega) = 2i\left(k_2^2 - k_1^2\right)\sin(k_2 L)/G, \tag{26e}$$

where $k_2$, $k_e$ and $k_1$ are wavenumbers of the Stoneley wave propagating in the porous formation, the equivalent elastic formation and the elastic formation, respectively; $v_{se}$ and $v_{s1}$ are the shear velocities of the porous formation and the elastic formation, respectively, and the symbol $D$ is the diffusion rate of pore fluid.

At a low-frequency limit, fluid motion in the pore occurs mainly as a slow-wave and is affected by the elasticity of the porous formation frame. For calculation convenience, the simplified theory ignores the elastic effect of the solid frame and only considers the displacement of the pore fluid; therefore, it ignores the second item ($\omega^2\rho_f\mathbf{u}$) in formula (1). However, it is necessary to consider the elastic effect in a porous formation with limited stiffness. Chang *et al.* (1988) approximated the elastic effect by correcting the diffusion rate, $D$, but for a smaller stiffnesses or more permeable formation, the error of the simplified theory is also relatively large even when $D$ is corrected

### 5.2 Porous formations with different elastic frame

To investigate the effects of the elastic frame, we use the FDTD method to simulate four porous formations with different elastic frames. The parameters of these formations are listed in Table 1. These porous formations have porosity $\phi = 0.3$, permeability $\kappa_0 = 2$ Darcy and centre frequency $f_0 = 2.2$ kHz. For the convenience of comparison, the formation thickness is considered to be infinite. Due to sampling time limitations, if the formation is thick enough (more than a few metres), the receiver can only receive the reflected waves produced by the lower surface of the porous formation, and the reflected waves are the same as those produced by an infinitely thick porous formation.

Fig. 4 shows the reflected Stoneley waves generated by four different porous formations. The waveform also represents the fluid pressure $p$ in the borehole. The frames of these four porous formations in Figs 4(a)–(d) correspond to the Frames 1–4 listed in Table 1, respectively. Elastic formations sandwiching these four porous formations are the same, and material parameters of these elastic formations are the same as those of Frame 2 listed in Table 1. The amplitudes of reflected Stoneley waves in Figs 4(a)–(c) are very similar and are significantly smaller than that of reflected Stoneley waves in Fig. 4(d). There is an obvious decrease in the amplitudes of the transmitted Stoneley waves, and the smallest amplitude is found in Fig. 4(d).

Stoneley waves propagating in a borehole with no associated porous formation are then simulated to get direct waves. If direct waves are subtracted from the waves in Fig. 4 reflected waves can be obtained. The frequency spectra of direct and reflected waves can be obtained using the Fourier transform method. The reflection coefficient of Stoneley wave near the elastic–porous interface will be abnormal, the axial distance of abnormal area is related to the size of borehole radius $a$ (Alexandrov *et al.* 2007). By analysing the frequency spectra of Stoneley wave, we find that when the distance between receiver and interface is more than $1.5a$, the spectra of reflected Stoneley wave recorded by different receivers is almost the same. Therefore, we select Stoneley waves recorded by the receiver with a distance of 1.8 m from the source (the distance between the receiver and the interface is about $2a$). The ratio of the spectra of reflected Stoneley wave to the spectra of direct Stoneley wave is the reflection coefficient of Stoneley wave in the frequency domain.

The absolute values of reflection coefficients in the frequency domain, $|r|$, calculated from waveforms of Figs 4(a)–(d) are shown in Figs 5(a)–(d), respectively. The dashed curves represent $|r|$ obtained using the FDTD method, and the solid curves are $|r|$ calculated using the simplified theory. With an increase in frequency, there is a gradual reduction in the reflection coefficients obtained using both the FDTD method and the simplified theory. However, with a decrease in porous formation frame stiffness, there is a gradual increase in the reflection coefficients calculated by these two methods. This occurs because of the greater difference between the Stoneley wavenumbers of the porous formation with a smaller stiffness and those of the elastic formation is larger.

The $|r|$ calculated by the FDTD method is represented by r_FD, and the $|r|$ obtained by the simplified theory is shown as r_S. For the rigid case, the associated frame is that of Frame 1 listed in Table 1, and r_FD is almost identical to r_S, as shown in Fig. 5(a). For Frame 2, r_FD is slightly less than r_S; this result shows that the stiffness of the formation frame is very large compared to the fluid modulus, the slow wave and fast wave are no longer coupled, therefore r_S is accurate.

For Frames 3 and 4, r_FD and r_S are very close when the frequency is less than 700 Hz. This result occurs at very low frequencies, because $\rho_f\omega^2 u \sim 0$, r_S is accurate. However, when the frequency is higher than 700 Hz, r_FD is significantly smaller than r_S, and the difference between them increases with an increase in the frequency. It is known that the differences are caused by a rise in the elasticity or compressibility of the frame: when the compressibility of the formation frame is equivalent to the compressibility of the pore fluid, the coupling between the slow wave and the fast wave is strengthened. This coupling causes the reflection of the Stoneley wave to be more significantly affected by formation elasticity. Thus, there is a greater difference between r_FD and r_S as the stiffness of the frame decreases.

Fig. 6 shows the wavefields of the Stoneley wave reflection by four different porous formations at the instant of 2.5 ms. The wavefield is the field of the normal stress component $\tau_{rr}$. Frames of these four porous formations are Frames 1–4 list in Table 1, respectively. The source is located at $z = 500$ cm and $r = 0$ cm, the black dashed line represents the borehole wall, and the porous formation is located at $z < 300$ cm. There is an evident gradual increase in the energy of the reflected Stoneley wave with decrease in formation rigidity, and the fast waves are not found in the porous formation with hard frame but exist in the porous formation with soft frame. This also indicates that coupling between the fast wave and the slow wave becomes significant when the compressibility of the formation is equivalent to the compressibility of the pore fluid.

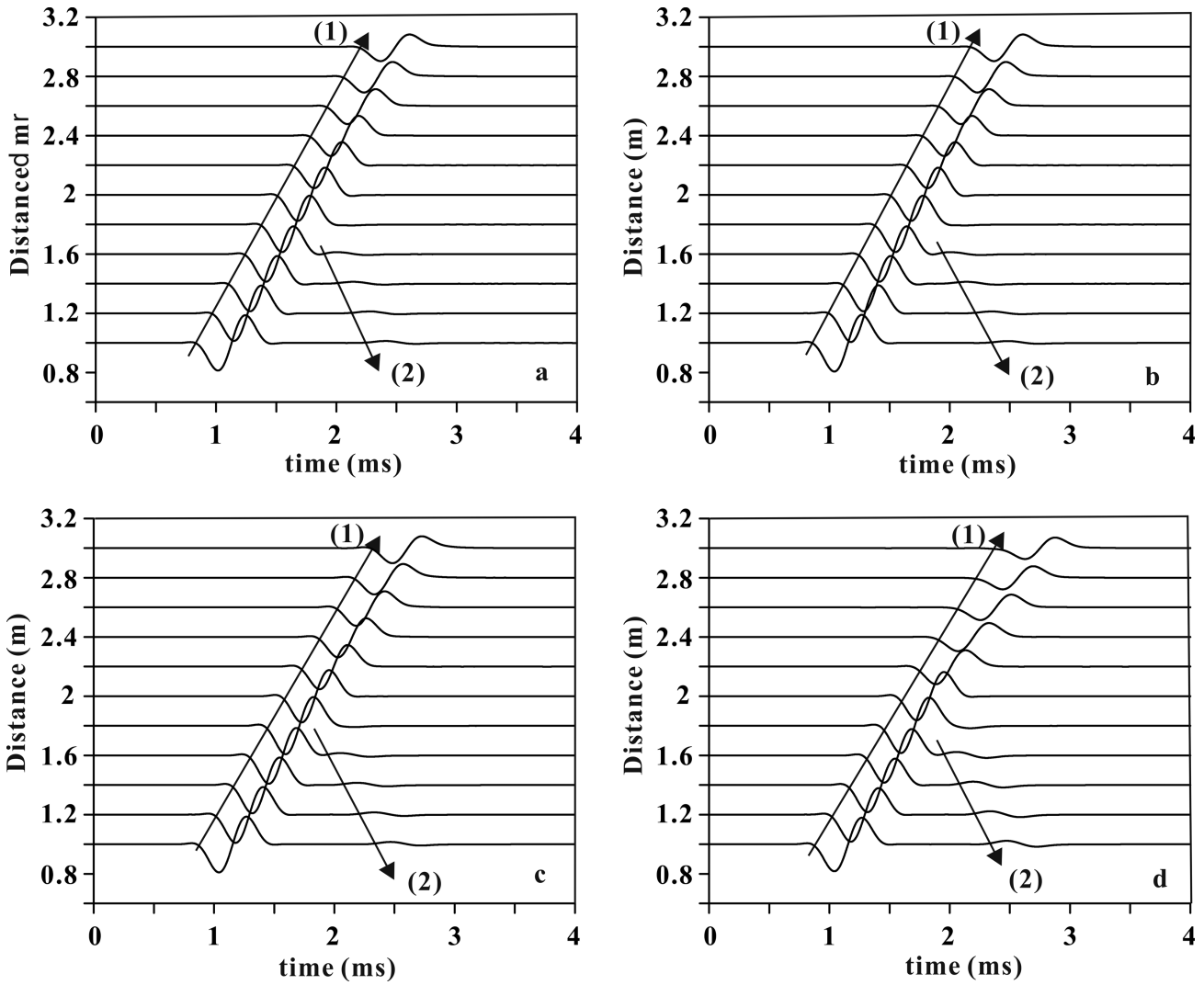


**Figure 4.** Reflected Stoneley waves generated by four different porous formations. The frames of porous formations in Figs 4(a)–(d) correspond to the Frames 1–4 in Table 1. Number (1) and number (2) represent the direct Stoneley wave and reflected Stoneley wave, respectively. The longitudinal axis represents the distance from the receiver to the source. The source distance of the interface between the porous formation and the elastic formation is 2 m.

### 5.3 Porous formations with different porosities and permeabilitie

We then compare the Stoneley wave reflection coefficients calculated by the two methods for porous formations with different permeabilities. We simulate three porous formations with different porosities and permeabilities, and the thicknesses of these formations are also assumed to be infinite. Again, these porous formations have the same frame elastic modulus. The $K_b$ and $N$ of the frame are 5.6467 and 6.16 GPa, respectively; density, $\rho$, of these porous formations is 1850 kg m$^{-3}$, and $K_s$ is 8.0667 $\times$ 10$^9$ GPa. These formations are also hard formations, but they have little stiffness. The porosity, $\phi$, and static permeability, $\kappa_0$, of these porous formations are listed in Table 2, and the elastic formation is the Frame 2 listed in Table 1.

Fig. 7 shows a comparison between the reflection coefficients obtained using these two methods for the different permeable porous formations. The dashed curves and solid curves represent r_FD and r_S, respectively, and the curves a, b and c denote the reflection coefficients of Formation a, Formation b and Formation c, respectively. Again, the reflection coefficients obtained using these two methods match well at low frequencies, but r_FD is obviously less than r_S. At a frequency of 4000 Hz, the differences between r_FD and r_S in Formation a, b and c are 0.0274, 0.0231 and 0.0162, respectively. This result indicates that the effect of frame elasticity on pore fluid movement is enhanced, and this difference is caused by the coupling between solid motion and fluid movement becoming significant with a decrease in the porosity and permeability of the formation.

### 5.4 Stoneley wave reflection of corrected simplified theory

To improve the accuracy of the simplified theory, a simple semi-empirical and semi-theoretical approach can be used to calibrate the effects of formation elasticity (Tang & Cheng 2004). This modified simplified theory considers the effect of borehole wall elasticity on acoustic

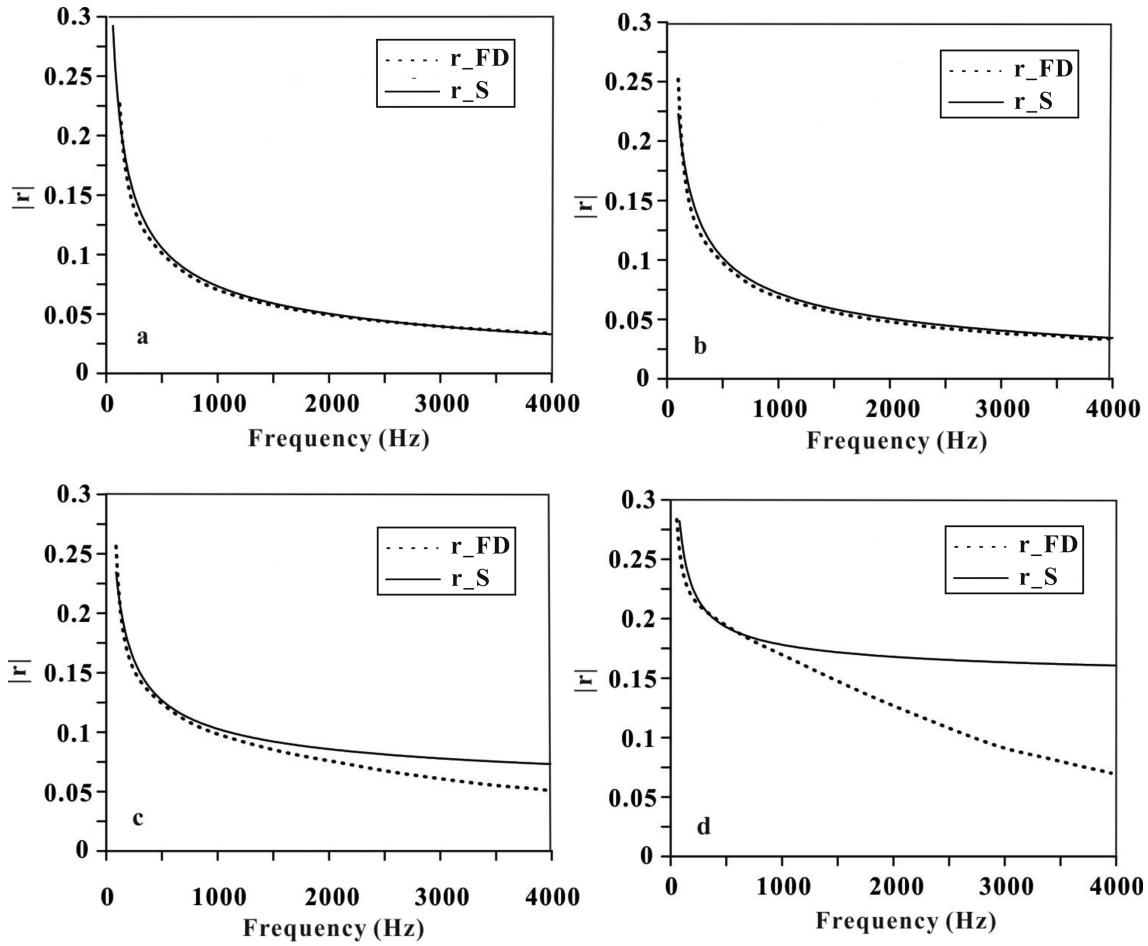


**Figure 5.** Reflection coefficients of Stoneley waves generated by four porous formations with different frames. The dashed curves represent $|r|$ obtained using the FD method, and the solid curves are $|r|$ calculated using the simplified theory.

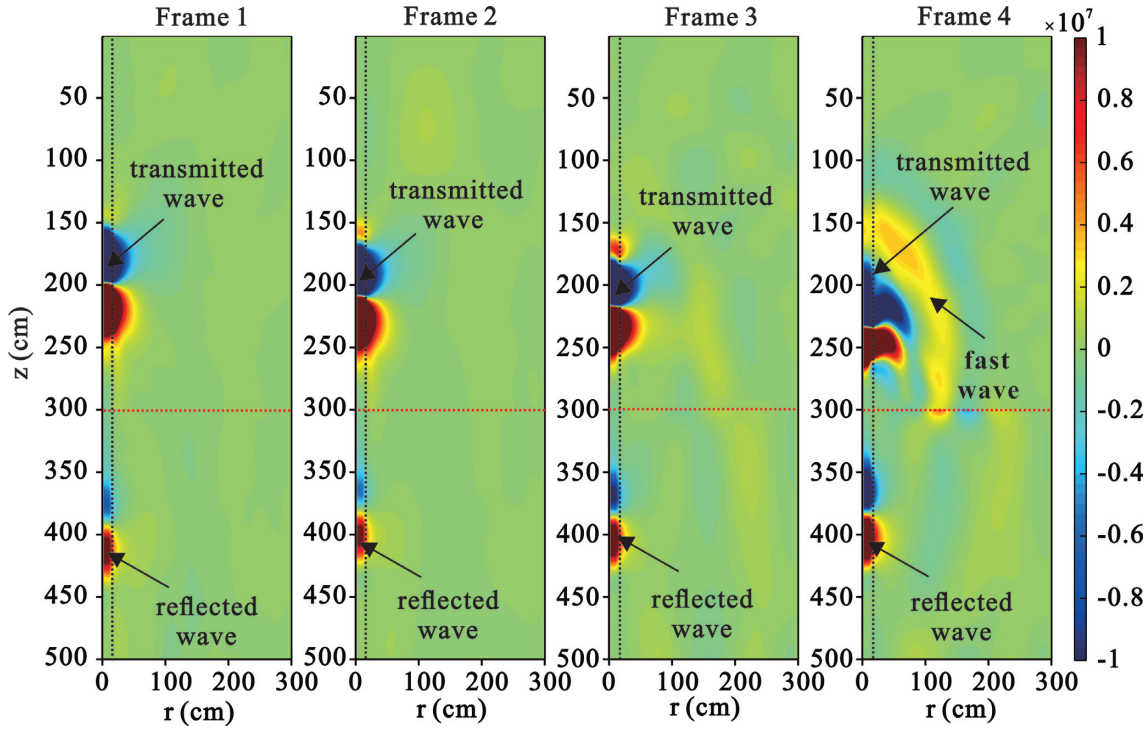


**Figure 6.** Wavefield of Stoneley wave reflection by four porous formations with different frames at instant of 2.5 ms. The source is located at $z = 500$ cm and $r = 0$ cm; and porous formation is located at $z < 300$ cm. The black dashed line represents the borehole wall, the red dashed line represents the interface between the porous formation and elastic formation.

**Table 2.** Porosities and permeabilities of different porous formations with same frame elastic modulus. $K_b$ and $N$ of the frame are 5.6467 and 6.16 GPa, respectively; density, $\rho$, of these porous formations is 1850 kg m$^{-3}$; and $K_s$ is 8.0667 $\times$ 10$^9$ GPa.

| | $\phi$ | $\kappa_0$ Darcy |
|---|---|---|
| Formation a | 0.1 | 0.2 |
| Formation b | 0.2 | 0.8 |
| Formation c | 0.3 | 2 |

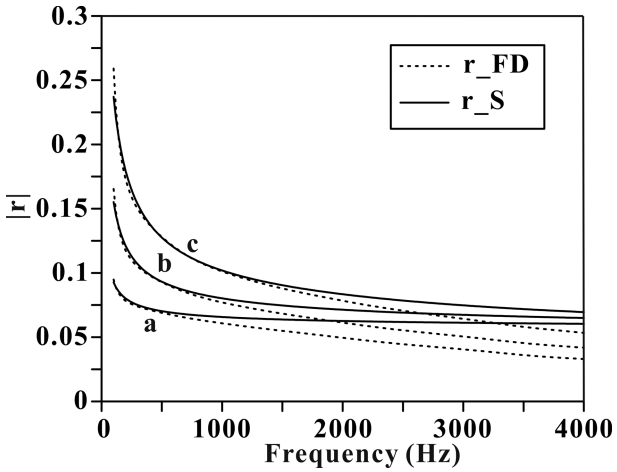


**Figure 7.** Comparison between reflection coefficients obtained by FD method and simplified theory for porous formations with different porosities and permeabilities. The curves a, b and c denote reflection coefficients of Formation a, b and c, respectively.

response in boreholes. The borehole compliance (BC) characterizes the compliance of the borehole wall with respect to the borehole fluid (Tang *et al.* 1991b), and it is defined by the following dimensionless parameter (Tang & Cheng 2004).

$$\mathrm{BC} = f_e a \frac{I_1(f_e a)}{I_0(f_e a)}, \tag{27}$$

where $f_e = \sqrt{k_e^2 - \omega^2/v_f^2}$, is the corresponding radial wavenumber of Stoneley waves in the equivalent formation. Tang & Cheng (2004) found a simple correction for formation elasticity by dividing, in eq. (26a), the second term under the square root sign by a factor of $1 + \mathrm{BC}^{v_{se}/v_f}$. According to the simulation results of the FD method and referring to the simple correction of Tang & Cheng (2004), a simple method to correct formation elasticity can be obtained by using the parameter BC. However, the effect of frame elasticity is very large due to the fast wave in the soft formation. We therefore revise the formula (26a) so that it is applicable for hard formation and soft formation cases. For hard formations, the modified formula is as follows:

$$k_2 = \sqrt{k_e^2/\left(1 + 0.15\mathrm{BC}^{v_f/v_{se}}\right) + \frac{2i\rho_f\omega\kappa(\omega)}{a\eta\left(1 + \mathrm{BC}^{v_{se}/v_f}\right)}\sqrt{\frac{-i\omega}{D}}\frac{K_1\left(a\sqrt{-i\omega/D}\right)}{K_0\left(a\sqrt{-i\omega/D}\right)}}, \tag{28}$$

and for the soft formation, the modified formula is

$$k_2 = \sqrt{k_e^2 \Bigg/ \left(1 + 0.4\mathrm{BC}^{v_f/v_{se}}\right) + \frac{2i\rho\omega\kappa(\omega)}{a\eta\left(1 + 6\mathrm{BC}^{v_f/v_{se}}\right)}\sqrt{\frac{-i\omega}{D}}\frac{K_1\left(a\sqrt{-i\omega/D}\right)}{K_2\left(a\sqrt{-i\omega/D}\right)}}. \tag{29}$$

Fig. 8 shows the Stoneley wave reflection coefficient calculated using the modified simplified theory. In Figs 8(a) and (b), the formation is hard and the formation frame is Frame 3, as shown in Table 1, whereas in Figs 8(c) and (d), the formation is soft and the formation frame is Frame 4, as shown in Table 1. The formation has a porosity of 0.3 and a permeability of 2 Darcy in Figs 8(a) and (c). The porosity and permeability of the formation in Figs 8(b) and (d) are 0.2 and 0.8 Darcy, respectively. For the hard formation, modified results are very close to the FD results. However, for the soft formation, the differences between the Stoneley wave reflection coefficient calculated by the modified simplified theory and that obtained by the Biot's theory in the low-frequency limit are obviously reduced. This indicates that after BC correction, the coincidence degree between the simplified theory and the Biot's theory is improved. Therefore, by using this simple modified method, the reflection of Stoneley waves in the porous formation can be rapidly simulated by employing the simplified theory.

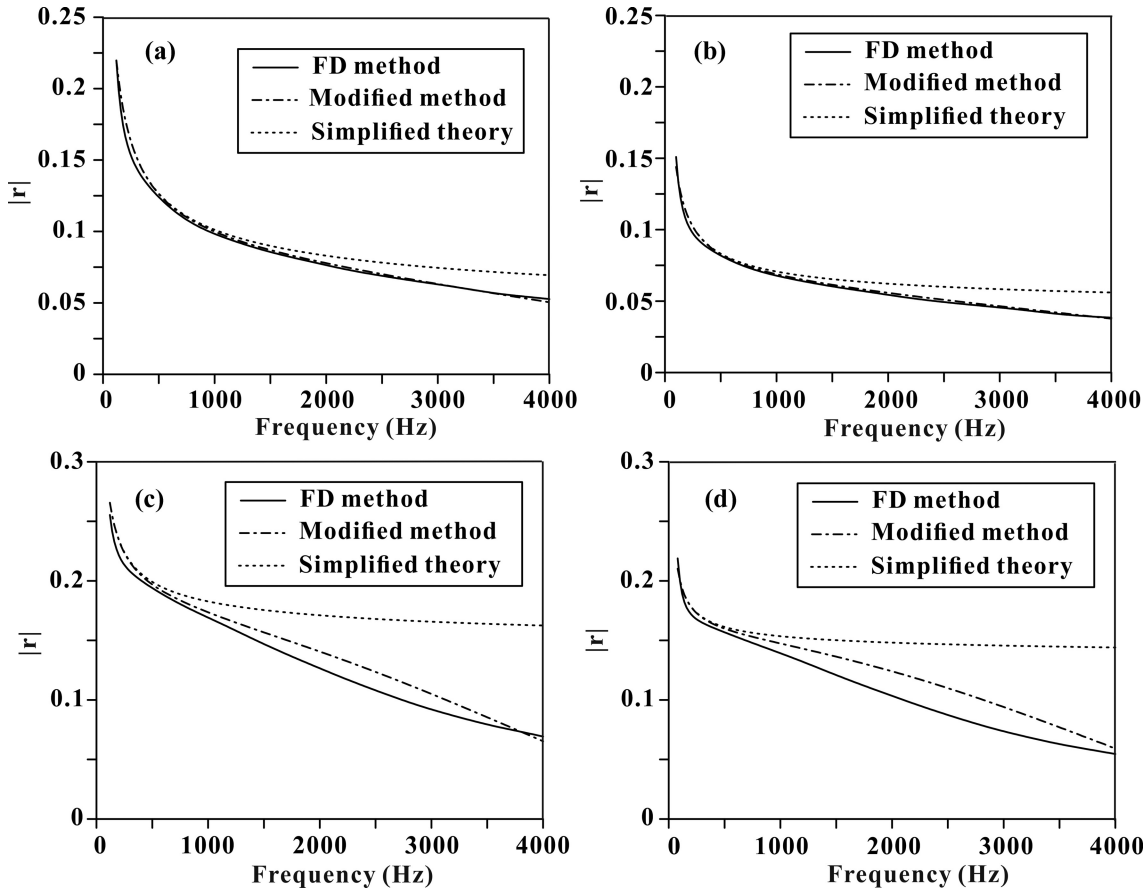


**Figure 8.** Stoneley wave reflection coefficient calculated using corrected simplified theory. The dashed curves represent $|r|$ obtained using the simplified theory; the solid curves are $|r|$ calculated using the FD method and the dot-dashed curves are $|r|$ calculated using the corrected simplified theory.

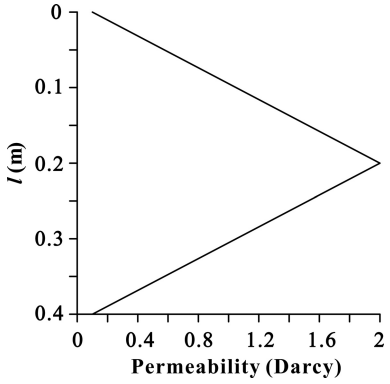


**Figure 9.** Model of permeability changes in axial direction. The variate, $l$, represents depth; depth $l = 0$ m and $l = 0.4$ m represent top and bottom of formation, respectively.

## 6 Stoneley wave reflection of heterogeneous porous formations

### 6.1 Model of permeability changes in axial direction

The simplified theory only calculates the reflection coefficient of Stoneley waves for a homogeneous porous formation. However, formation permeability is not a constant, and it gradually changes with depth, where it first increases and then decreases. We use the FDTD method to simulate the effect of changes in permeability in the axial direction on Stoneley wave reflection.

We assume that the permeability of the porous formation in this model varies linearly with depth. As shown in Fig. 9, the porous formation thickness, $L$, is 0.4 m; porosity, $\phi$, is 0.3; the static permeability, $\kappa_0$, at the top ($l = 0$ m) and bottom ($l = 0.4$ m) of the formation is 0.1 Darcy and $\kappa_0$ in the middle ($l = 0.2$ m) of the formation is 2 Darcy. With the increase in depth, $\kappa_0$ of the formation increases to 2 Darcy and then decreases to 0.1 Darcy. We also simulate two homogeneous porous formations that have $\kappa_0$ values of 0.1 and 2 Darcy, respectively. The

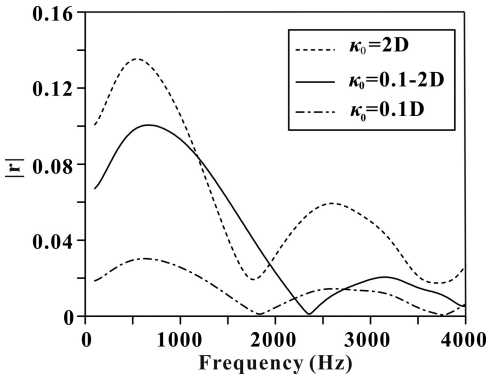


**Figure 10.** Reflection coefficient of model with changes in permeability in axial direction. The dashed curve represents $|r|$ of homogeneous formation with $\kappa_0 = 2$ Darcy, the dot-dashed curve represents $|r|$ of homogeneous formation with $\kappa_0 = 0.1$ Darcy and the solid curve represents $|r|$ of model for permeability changes in axial direction.

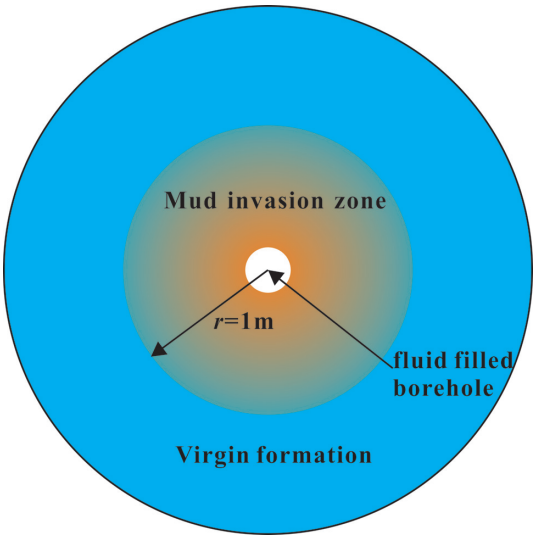


**Figure 11.** Geometry of mud invasion model. The radius, $r$, of the mud invasion zone is 0.1 m.

thicknesses and porosities of these two formations are the same as that of the model. The reflection coefficient of the model is then compared with that of the homogeneous permeable formations.

Fig. 10 shows the difference between the reflection coefficient of the model and that of the homogeneous porous formation, where it is evident that the peaks of the three reflection coefficient curves are different. The peak value of this model is greater than that of the porous formation with $\kappa_0 = 0.1$ Darcy but is less than that of the porous formation with $\kappa_0 = 2$ Darcy. This result occurs because the range of $\kappa_0$ is 0.1 to 2 Darcy for this model and reflected Stoneley waves are generated by all the axial permeability of the formation. The reflection waves generated by the upper and lower surface of the porous formation overlap with each other, which results in a series of peaks in the curves. Although the peak intervals, $\Delta f$, of the reflection coefficient curves of the homogeneous porous formation are the same, the peak interval of this model is greater. According to the relationship $\Delta f \cong V_{st}/L$ (Tang 1990), the thickness of this model appears to be smaller. Permeability changes in axial direction also produced reflected Stoneley waves, and the reflected wave energy is greater than that generated at both ends of this model; whereas in the homogeneous porous formation, reflection waves are produced only at both ends of the formation. Therefore, the peak interval of the reflection coefficient curve is increased in this model.

### 6.2 Model of mud invasion

During drilling, mud filtrate in a borehole penetrates into the porous formation, which causes the water within the pore to be squeezed out. Pore water near the borehole can be almost completely replaced (or mixed with mud) in the pores. If the viscosity of the mud is different from that of the virgin pore water, the fluid mobility, $\kappa_0/\eta$, in the formation may therefore change. There is less mud filtrate with distance from the wall, which leads to change in pore fluid mobility along the radial direction. Therefore, we use a model of fluid viscosity with radial variation to simulate the effect of mud invasion.

Fig. 11 shows the geometry of the mud invasion model. The virgin pore fluid viscosity $\eta_0$ is $10^{-3}$ Pa · s. We consider two formations invaded by mud; in both formations, the viscosity of the fluid varies linearly from the borehole wall to the radius $r = 1$ m. As shown in Table 3,

**Table 3.** Pore fluid viscosity of mud invasion models.

| | $\eta$ ($\eta_0$) | $\kappa_0/\eta$ ($\kappa_0/\eta_0$) |
|---|---|---|
| Formation 1 | 0.1–1 | 10–1 |
| Formation 2 | 10–1 | 0.1–1 |
| Formation 3 | 0.1 | 10 |
| Formation 4 | 10 | 0.1 |

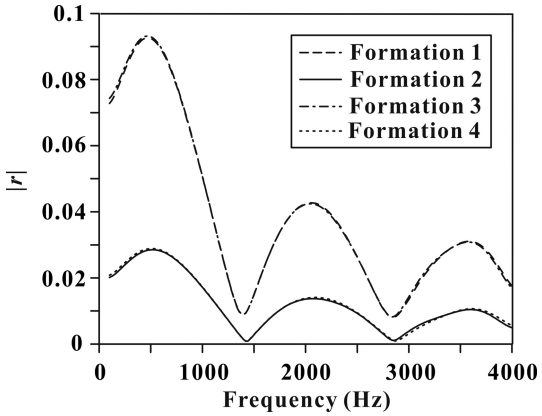


**Figure 12.** Stoneley wave reflection coefficient of mud invasion models. Fluid viscosity, $\eta$, in Formation 1 is increased from 0.1 $\eta_0$ to $\eta_0$, the $\eta$ while that in Formation 2 is reduced from 10 $\eta_0$ to $\eta_0$ and that in Formation 3 and Formation 4 are $0.1\eta_0$ and $10\eta_0$, respectively.

the fluid viscosity, $\eta$, in Formation 1 is increased from 0.1 $\eta_0$ to $\eta_0$, whereas that in Formation 2 is reduced from 10 $\eta_0$ to $\eta_0$. Two homogeneous porous formations (Formation 3 and Formation 4) are also simulated for comparing with the mud invasion model. These two formations have fluid viscosities $0.1\eta_0$ and $10\eta_0$, respectively; the porosity, $\phi$, is 0.2; virgin formation permeability, $\kappa_0$, is 1 Darcy; and formation thickness, $L$, is 0.5 m.

Fig. 12 shows the Stoneley wave reflection coefficients of the mud invasion models. The reflection coefficient of Formation 1 is almost the same as that of Formation 3, while that of Formation 2 is almost the same as that of Formation 4. The fluid viscosity of Formation 3 (Formation 4) is the same as that of Formation 1 (Formation 2) at the borehole wall. As the depth at which the fluid is flowing into the formation is very small, the reflection coefficient of the mud invasion model is very close to that of the viscosity invariant model. These results show that the reflection coefficient of the mud invasion model is mainly affected by the viscosity of the formation fluid near the borehole wall, and the same results would be obtained if the viscosity of the fluid is constant and the permeability of the formation changes linearly. Therefore, the Stoneley wave reflection coefficient is mainly sensitive to fluid mobility near the borehole wall.

## 7 CONCLUSION

Based on the Boit's theory in the low-frequency limit, the FDTD method was used to simulate the Stoneley wave reflection from a porous formation in the borehole. Taylor expansion was used to approximate dynamic permeability in the low-frequency limit and dynamic permeability was then applied to the FDTD method. Results show a good match between Stoneley waves simulated by the FDTD method and those simulated by the RAI method, which verifies the FDTD method.

The reflection coefficients of the FDTD method are compared with that of the simplified theory and are found to be very similar when the porous formation is much less compressible than the water. In this case, the use of simplified theory is effective. However, when the compressibility of the formation is equivalent to the fluid, the reflection coefficient obtained by the simplified theory is greater, because the coupling between fluid motion and solid motion is ignored in the simplified theory at high frequencies. In addition, the difference between the FDTD method and the simplified theory becomes greater because of the strengthening of the coupling when the porosity and permeability of the formation is lower. In these cases, the effect of the frame elasticity cannot be ignored. The simulation using the FDTD method provides results that are more accurate and does not take much time (in approximately 14 s). The simple correction scheme can be used to incorporate the effects of formation elasticity by using the parameter BC. The modified simplified theory improves the calculation accuracy of Stoneley wave reflection coefficient and thus facilitates the application of Biot's theory.

The FDTD method can also be used to simulate the effect of heterogeneous permeable porous formations on Stoneley wave reflection. The reflection coefficients of heterogeneous permeable formations were compared with those of homogeneous permeable formations. Results show that reflected Stoneley waves are generated by all axial permeabilities of the formation, and there is an increase in the peak interval of the reflection coefficient curve due to the slow change in permeability in the axial direction. Even with a change in the mobility of the formation fluid in a radial direction, the Stoneley wave reflection was mainly affected by fluid mobility near the borehole wall. Understanding

the effects of a porous formation on Stoneley wave reflection is beneficial for inverting the parameters of a porous formation when using reflected Stoneley waves obtained from acoustic logging data.

## ACKNOWLEDGEMENTS

The work described in this paper is supported by the National Natural Science Foundation of China (No.41874135).

## REFERENCES

Alexandrov, D., Kashtan, B.M., Bakulin, A. & Ziatdinov, S., 2007. Tubewave reflections in cased boreholes, in *69th Annual Conference and Exhibition, EAGE, Extended Abstracts,* EAGE, Houten, p. P097.

Alford, R.M., Kelly, K.R. & Boore, D.M., 1974. Accuracy of finite-difference modeling of the acoustic wave equation, *Geophysics,* **39**(6), 834–842.

Auriault, J., Borne, L. & Chambon, R., 1985. Dynamics of porous saturated media, checking of the generalized law of Darcy, *J. acoust. Soc. Am.,* **77**(5), 1641–1650.

Bakulin, A., Gurevich, B., Ciz, R. & Ziatdinov, S., 2005. Tube-wave reflection from a porous permeable layer with an idealized perforation , in *SEG Technical Program Expanded Abstracts,* Vol. **24,** SEG, Houston, pp. 2668.

Biot, M.A., 1956a, Theory of propagation of elastic waves in a fluid-saturated porous solid, I: low frequency range, *J. acoust. Soc. Am.,* **28,** 168–178.

Biot, M.A., 1956b, Theory of propagation of elastic waves in a fluid-saturated porous solid, II: higher frequency range, *J. acoust. Soc. Am.,* **28,** 179–191.

Biot, M.A., 1962, Mechanics of deformation and acoustic propagation in porous media, *J. Appl. Phys.,* **33**(4), 1482–1498.

Chang, H.W. & Randall, C.J., 1988, Finite-difference time-domain modeling of elastic wave propagation in the cylindrical coordinate system, in *IEEE 1988 Ultrasonics Symposium Proceedings,* pp. 397–402, IEEE, Piscataway.

Chang, S.K., Liu, H.L. & Johnson, D.L., 1988, Low frequency tube waves in permeable rocks, *Geophysics,* **53,** 519–527.

Cheng, C.H., Zhang, J. & Burns, D.R., 1987, Effects of *in-situ* permeability on the propagation of Stoneley (tube) waves in a borehole, *Geophysics,* **52,** 1279–1289.

Dai, N., Vafidis, A. & Kanasewich, E.R., 1995, Wave propagation in heterogeneous, porous media: a velocity-stress, finite-difference method, *Geophysics,* **60**(2), 327–340.

Graves, R.W., 1996. Simulating seismic wave propagation in 3D elastic media using staggered-grid finite differences, *Bull. seism. Soc. Am.,* **86**(4), 1091–1106.

Guan, W. & Hu, H., 2008. Finite-difference modeling of the electroseismic logging in a fluid-saturated porous formation, *J. Comput. Phys.,* **227**(11), 5633–5648.

Guan, W., Hu, H. & He, X., 2009. Finite-difference modeling of the monopole acoustic logs in a horizontally stratified porous formation, *J. acoust. Soc. Am.,* **125**(4), 1942–1950.

Guan, W. & Hu, H., 2011, The parameter averaging technique in finite-difference modeling of elastic waves in combined structures with solid, fluid and porous subregions, *Commun. Comput. Phys.,* **10**(3), 695–715.

He, X., Wang, X. & Chen, H., 2012, 3D finite difference simulations of acoustic logs in tilted layered porous formations, *J. Comput. Acoust.,* **20**(02), 1240009.

He, X., Hu, H. & Wang, X., 2013. Finite difference modelling of dipole acoustic logs in a poroelastic formation with anisotropic permeability, *Geophys. J. Int.,* **192**(1), 359–374.

Johnson, D.L., Koplik, J. & Dashen, R., 1987, Theory of dynamic permeability and tortuosity in fluid-saturated porous media, *J. Fluid Mech.,* **176,** 379–402.

Karpfinger, F., Gurevich, B., Valero, H.P., Bakulin, A. & Sinha, B., 2010, Tube wave signatures in cylindrically layered poroelastic media computed with spectral method, *Geophys. J. Int.,* **183**(2), 1005–1013.

Kristek, J., Moczo, P., Chaljub, E. & Kristekova, M., 2017. An orthorhombic representation of a heterogeneous medium for the finite-difference modelling of seismic wave propagation, *Geophys. J. Int.,* **208,** 1250–1264.

Masson, Y.J., Pride, S.R. & Nihei, K.T., 2006. FDTD modeling of Biot's poroelastic equations at seismic frequencies, *J. geophys. Res.,* **111**(B10), doi:10.1029/2006JB004366.

Moczo, P., Kristek, J., Vavrycuk, V., Archuleta, R.J. & Halada, L., 2002. 3D heterogeneous staggered-grid finite-difference modeling of seismic motion with volume harmonic and arithmetic averaging of elastic moduli and densities, *Bull. seism. Soc. Am.,* **92**(8), 3042–3066.

Moczo, P., Kristek, J. & Galis, M., 2014. *The Finite-Difference Modelling of Earthquake Motions: Waves and Ruptures,* Cambridge University Press.

Moczo, P., Gregor, D., Kristek, J. & Puente, J.D.L., 2019. A discrete representation of material heterogeneity for the finite-difference modelling of seismic wave propagation in a poroelastic medium, *Geophys. J. Int.,* **216**(2), 1072–1099.

Parra, J.O. & Xu, P., 1994. Dispersion and attenuation of acoustic guided waves in layered fluid-filled porous media, *J. acoust. Soc. Am.,* **95**(1), 91–98.

Randall, C.J., Scheibner, D.J. & Wu, P.T., 1991. Multipole borehole acoustic waveforms: synthetic logs with beds and borehole washouts, *Geophysics,* **56**(11), 1757–1769.

Rosenbaum, J.H., 1974, Synthetic microseismograms: logging in porous formations, *Geophysics,* **39,** 14–32.

Schmitt, D.P., 1988. Effects of radial layering when logging in saturated porous formations, *J. acoust. Soc. Am.,* **84**(6), 2200–2214.

Stephan, R.A., Cardo-Casas, F. & Cheng, C.H., 1985. Finite-difference synthetic acoustic logs, *Geophysics,* **50,** 1588–1609.

Tang, X.M., 1990. *Acoustic Logging in Fractured and Porous Formations,* Ph.D. thesis., Massachusetts Institute of Technology.

Tang, X.M., Cheng, C.H. & Toksöz, M.N., 1991a, Dynamic permeability and borehole stoneley waves: a simplified Biot–Rosenbaum model, *J. acoust. Soc. Am.,* **90**(3), 1632–1646.

Tang, X.M., Cheng, C.H. & Toksöz, M.N., 1991b. Stoneley-wave propagation in a fluid-filled borehole with a vertical fracture, *Geophysics,* **56**(4), 447–460.

Tang, X.M. & Cheng, C.H., 1993. Borehole Stoneley wave propagation across permeable fractures, *Geophys. Prospect.,* **41**(2), 165–187.

Tang, X. & Cheng, C.H., 1996. Fast inversion of formation permeability from Stoneley wave logs using a simplified Biot-Rosenbaum model, *Geophysics,* **61**(3), 639–645.

Tang, X.M. & Cheng, C.H., 2004. *Quantitative Borehole Acoustic Methods,* Elsevier Science Publishing Co., Inc.

Tsang, L. & Rader, D., 1979. Numerical evaluation of the transient acoustic waveform due to a point source in a fluid-filled borehole, *Geophysics,* **44**(10), 1706.

Virieux, J., 1986. P-sv wave propagation in heterogeneous media; velocity-stress finite-difference method, *Geophysics,* **49**(11), 1933–1942.

Wang, T. & Tang, X., 2003. Finite-difference modeling of elastic wave propagation: a nonsplitting perfectly matched layer approach, *Geophysics,* **68**(5), 1749–1755.

Zeng, Y.Q., He, J.Q. & Liu, Q.H., 2001. The application of the perfectly matched layer in numerical modeling of wave propagation in poroelastic media, *Geophysics,* **66**(4), 1258.

Zeng, Y.Q. & Liu, Q.H., 2001. A staggered-grid finite-difference method with perfectly matched layers for poroelastic wave equations, *J. acoust. Soc. Am.,* **109**(6), 2571–2580.

Zhao, X., Toksöz, M.N. & Cheng, C.H., 1993. Stoneley wave propagation in heterogeneous permeable porous formations, *SEG Technical Program Expanded Abstracts,* pp. 1396, SEG, Tulsa.

Zhu, X. & McMechan, G.A., 1991. Numerical simulation of seismic responses of poroelastic reservoirs using Biot theory, *Geophysics,* **56,** 328–339.

## APPENDIX: THE PARAMETER AVERAGING TECHNIQUE

Averaged parameters with superscript *Ar* at the location $(k, j + 1/2)$ are the averages of the material parameters at the locations $(k + 1/2, j + 1/2)$ and $(k-1/2, j + 1/2)$, such as

$$\rho^{Ar}_{(k,j+1/2)} = 0.5\left(\rho_{(k-1/2,j+1/2)} + \rho_{(k+1/2,j+1/2)}\right). \tag{A1}$$

Averaged parameters with superscript *Az* at the location $(k + 1/2, j)$ are the averages of the material parameters at the locations $(k + 1/2, j + 1/2)$ and $(k + 1/2, j-1/2)$, such as

$$\rho^{Az}_{(k+1/2,j)} = 0.5\left(\rho_{(k+1/2,j-1/2)} + \rho_{(k+1/2,j+1/2)}\right). \tag{A2}$$

The harmonic mean $\mu^{\mathrm{H}}$ is defined as

$$\mu^{H}_{(k,j)} = 4/\left(\mu^{-1}_{(k-1/2,j-1/2)} + \mu^{-1}_{(k+1/2,j-1/2)} + \mu^{-1}_{(k-1/2,j+1/2)} + \mu^{-1}_{(k+1/2,j+1/2)}\right). \tag{A3}$$

At the interface of fluid-elastic or fluid-porous, $\mu^{H}_{(k,j)} = 0$ (Chang & Randall 1988).